Anita Penkova
Department of Aerospace & Mechanical Engineering,
University of Southern California,
Los Angeles, CA 90089-1453;
Saban Research Institute,
Children's Hospital Los Angeles,
Los Angeles, CA 90027

Rex Moats
Saban Research Institute,
Children's Hospital Los Angeles,
Los Angeles, CA 90027;
Department of Biomedical Engineering,
University of Southern California,
Los Angeles, CA 90089-1111

Mark S. Humayun
Department of Ophthalmology,
USC Roski Eye Institute,
Department of Integrative Anatomical Sciences,
Keck School of Medicine,
University of Southern California,
Los Angeles, CA 90033-4682;
Department of Biomedical Engineering,
University of Southern California,
Los Angeles, CA 90089-1111

Scott Fraser
Departments of Molecular and Computational Biology,
Dornsife College of Letters, Arts and Sciences,
University of Southern California,
Los Angeles, CA 90089-0371;
Department of Biomedical Engineering,
University of Southern California,
Los Angeles, CA 90089-1111;
Departments of Pediatrics, Ophthalmology, Radiology,
Keck School of Medicine,
University of Southern California,
Los Angeles, CA 90033-4682

Satwindar Singh Sadhal[1]
Department of Aerospace & Mechanical Engineering,
University of Southern California,
Los Angeles, CA 90089-1453;
Saban Research Institute,
Children's Hospital Los Angeles,
Los Angeles, CA 90027;
Department of Ophthalmology,
Keck School of Medicine,
University of Southern California,
Los Angeles, CA 90033-4682
e-mail: sadhal@usc.edu

Diffusive Transport in the Vitreous Humor: Experimental and Analytical Studies

In relation to intravitreal drug delivery, predictive mathematical models for drug transport are being developed, and to effectively implement these for retinal delivery, the information on biophysical properties of various ocular tissues is fundamentally important. It is therefore necessary to accurately measure the diffusion coefficient of drugs and drug surrogates in the vitreous humor. In this review, we present the studies conducted by various researchers on such measurements over the last several decades. These include imaging techniques (fluorescence and magnetic resonance imaging (MRI)) that make use of introducing a contrast agent or a labeled drug into the vitreous and tracking its diffusive movement at various time points. A predictive model for the same initial conditions when matched with the experimental measurements provides the diffusion coefficient, leading to results for various molecules ranging in size from approximately 0.1 to 160 kDa. For real drugs, the effectiveness of this system depends on the successful labeling of the drugs with suitable contrast agents such as fluorescein and gadolinium or manganese so that fluorescence or MR imagining could be conducted. Besides this technique, some work has been carried out using the diffusion apparatus for measuring permeation of a drug across an excised vitreous body from a donor chamber to the receptor by sampling assays from the chambers at various time intervals. This has the advantage of not requiring labeling but is otherwise more disruptive to the vitreous. Some success with nanoparticles has been achieved using dynamic light scattering (DLS), and presently, radioactive labeling is being explored. [DOI: 10.1115/1.4042297]

1 Introduction

For ocular drug delivery as a therapy for retinal diseases, the target is the posterior segment of the eye. The delivery to the retina has challenges that come about because of the various barriers which affect the drug concentration distribution [1]. Furthermore, a balanced delivery rate is highly desirable since low drug concentrations could be insufficient for the treatment, while high

[1]Corresponding author.
Contributed by the Heat Transfer Division of ASME for publication in the Journal of Heat Transfer. Manuscript received September 18, 2018; final manuscript received December 11, 2018; published online April 1, 2019. Assoc. Editor: Milind A. Jog.

concentrations could be toxic, depending on the specific drug and its toxicity. In order to predict delivery rates, detailed information about the transport mechanisms is necessary, and among the fundamental parameters in this regard is the diffusion coefficient of the vitreous humor. Accurate measurements of this parameter are necessary for developing algorithms that may be applied for predicting transport rates of various compounds for application to ocular drug delivery. This aspect for predictive modeling has been discussed in earlier publications [2–5], and we will not elaborate on that here. Also, we have discussed earlier [2] the need to isolate diffusion from convection since the processes are driven by different physical mechanisms, even though in a live eye these processes happen simultaneously. The focus therefore is on the diffusive transport and the measurement of the diffusion coefficient. There are clear challenges because the vitreous humor is a very delicate material and is subject to difficulties in handling.

To make scientific and translational progress in ocular drug delivery, deep understanding of the transport processes is necessary. To this end, quantification with mathematical modeling along with careful experimentation provides an avenue for such understanding. Over the last few decades, considerable progress has been made in the area of numerical modeling of ocular transport process [4–10]. On the experimental side, magnetic resonance imaging (MRI) has been particularly useful in providing insight into the transport processes following intravitreal injection [4,11,12]. For success in the numerical modeling effort, accurate measurement of the transport properties of the vitreous, particularly the diffusion coefficient, are fundamentally important, and this is the focus of the present review.

It should be noted that in a living eye, both diffusive and convective transport are present in the vitreous, and these processes take place together [13]. The two processes are driven by different physical mechanisms, diffusion by a concentration gradient, and convection by water flow [14–17], but it has been common to treat the combined effect with an "effective" diffusion coefficient. However, keeping the physics in sight, we shall treat the two processes as separate, and the present review focuses on pure diffusion. For the purpose of developing a comprehensive mathematical model transport in the eye, the values of the diffusion coefficient D may be used only to account for the diffusion aspect of the transport processes, and it is understood that other processes (such as convection) will need to be included for such a model.

There are several measurement techniques that have been developed over the last 30–40 years, some utilizing the whole eye and others using extracted vitreous. The methods have depended on imaging (fluorescence or magnetic resonance) as well as sampling of assays. Imaging techniques have the advantage of providing a snapshot of the concentration profile without having to extract the vitreous. In this regard, MRI is particularly useful since it provides the concentration over numerous slices of the subject eye. However, there are limitations because the drug for which the diffusion coefficient is being measured needs to be labeled with fluorescein or an MRI contrast agent and this can present difficulties for certain molecules. On the other hand, placing the vitreous into a short cylindrical chamber in contact with buffer-filled donor and receptor chambers [10], akin to an Ussing chamber, allows measurements of drug transport across the vitreous. However, the technique is intrusive, and the sampling of the buffers depletes the chambers and limits the number of time points. These and other techniques are discussed in detail in Sec. 2.

2 Measurement Techniques

As discussed in the Introduction, techniques where the whole eye (ex vivo or in vivo) is used, imaging has to be employed. The approach for such techniques consists of solving an inverse problem by introducing a contrast agent into the vitreous and imaging the progression of its spread in time. This spread is also modeled theoretically, based on the time-dependent diffusion equation, and a comparison of the model with the experiment (a least-squares best fit) can return the value of the unknown diffusion coefficient. We shall begin with a discussion on the fluorescence techniques.

2.1 Fluorescence-Based Imaging. Some of the pioneering work on the measurement of diffusion properties in ocular tissue has been conducted in studies by Maurice and coworkers [18–20] with the use of fluorescein as well as fluorescein-labeled dextran (FD). Garlick and Renkin [21] investigated the diffusion coefficients in water for various FD molecules with molecular weights ranging from 8.5 to 500 kDa. In Ref. [22], Maurice has interpolated these data and given the diffusion coefficient values for FD in water with molecular weights of 65 kDa and 167 kDa as 6.0×10^{-7} and 3.9×10^{-7} cm^2/s, respectively, and applied these values for diffusive transport in the rabbit vitreous. While in these studies [18–20,22] extensive diffusion characteristics in the vitreous have been experimentally studied, the main focus of these works has been on the permeability properties of the surrounding tissue and obtaining drug clearance time parameters (e.g., the loss coefficient k_v which has units of h^{-1}). Since there have been no measurements of the diffusion coefficient D reported therein but rather other prior measurements for diffusion in water have been relied upon, we shall not discuss these works in more detail.

Other early works on fluorescein include the investigation by Larsen et al. [23] on human eyes. They used fluorescein (reported molecular weight of 0.372 kDa) that was injected into the bloodstream and allowed to penetrate the vitreous through the blood-retinal barrier (BRB). The fluorescein concentration was measured along points on the axis of the eye and compared with the theoretical prediction based on the eye being approximated as a sphere, as shown in Fig. 1. The main intention of this work was the measurement of the permeability of the BRB, and the diffusion coefficient of the vitreous was an additional unknown in the system. For a spherical vitreous of radius R, the theoretical problem was stated in a spherical coordinate system:

Diffusion Equation

$$\frac{1}{D}\frac{\partial c}{\partial t} = \frac{\partial^2 c}{\partial r^2} + \frac{2}{r}\frac{\partial c}{\partial r}, \quad 0 \le r \le R \tag{1}$$

where $c(r,t)$ is the concentration distribution of fluorescein, D is the diffusion coefficient of fluorescein in the vitreous, and R is the radius of curvature of the posterior of the eye.

Boundary Conditions

At the center of the sphere

$$\left.\frac{\partial c}{\partial r}\right|_{r=0} = 0 \tag{2}$$

and at $r = R$, the mixed boundary condition was used due to the finite permeability P of the BRB, i.e.,

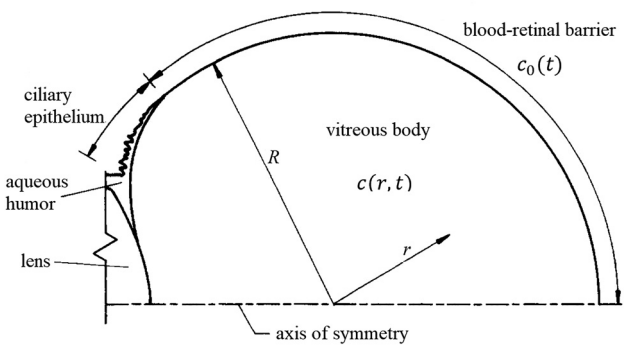

Fig. 1 Schematic of the section through the eye. The vitreous body is approximated as a sphere of radius *R*. The radial spherical coordinate is *r*. Adapted from Ref. [23], with permission from Springer Nature © 1983.

$$c(R,t) + \frac{D}{P}\frac{\partial c}{\partial r}\bigg|_{r=R} = c_0(t) \tag{3}$$

where $c_0(t)$ is the fluorescein concentration in the bloodstream based on the data provided by Lund-Andersen et al. [24] that of course decreases in time as the fluorescein clears. The solution to the set of Eqs. (1)–(3) was obtained by Laplace transform and the expression valid for short-time is given by [23]

$$c(r,t) \cong \int_0^t c_0(t-\tau)F(r,\tau)d\tau \tag{4}$$

where

$$F(r,\tau) = \frac{PR}{r\sqrt{D}}\left\{\frac{2}{\sqrt{\pi\tau}}e^{-\frac{R^2+r^2}{4D\tau}}\sinh\left(\frac{rR}{2D\tau}\right) - \lambda e^{\lambda^2\tau}\left[e^{\frac{\lambda(R-r)}{\sqrt{D}}}\operatorname{erfc}\left(\lambda\sqrt{\tau}+\frac{R-r}{\sqrt{4D\tau}}\right) - e^{\frac{\lambda(R+r)}{\sqrt{D}}} \times \operatorname{erfc}\left(\lambda\sqrt{\tau}+\frac{R+r}{\sqrt{4D\tau}}\right)\right]\right\} \tag{5}$$

with

$$\lambda = \frac{P}{\sqrt{D}} - \frac{\sqrt{D}}{R} \tag{6}$$

The authors dealt with real patients as fluorescein penetration from the BRB to the vitreous was tracked by the fluorophotometric technique. The concentration was determined as an average over a small volume spanned by the incident beam of blue light and the detector beam. Using the predicted concentration given by Eqs. (4)–(6) and the measured concentration, the sum of the squares of the differences of these was minimized while P and D were unknown. The least-squares best fit was used to deliver the unknowns. Figure 2 here represents an example of the experimental data along the axis of the eye and the theoretical best fit. In this particular case, the authors gave $P = 0.830 \times 10^{-6}$ cm/s and $D = 8.91 \times 10^{-6}$ cm^2/s. In a subsequent development by Lund-Andersen et al. [25], measurements were carried out with normal patients as well as those with diabetic retinopathy and macular edema. The results for the sample of six normal patients was reported as $P = (7.1 \pm 3.8) \times 10^{-7}$ cm/s and $D = (9.6 \pm 2.0) \times 10^{-6}$ cm^2/s. For the same number of diabetic patients, higher transport parameters were reported with average values $P = (1.1 \pm 0.4) \times 10^{-7}$ cm/s and $D = (7.4 \pm 3.4) \times 10^{-6}$ cm^2/s, indicating a very substantial increase in the permeability of the BRB.

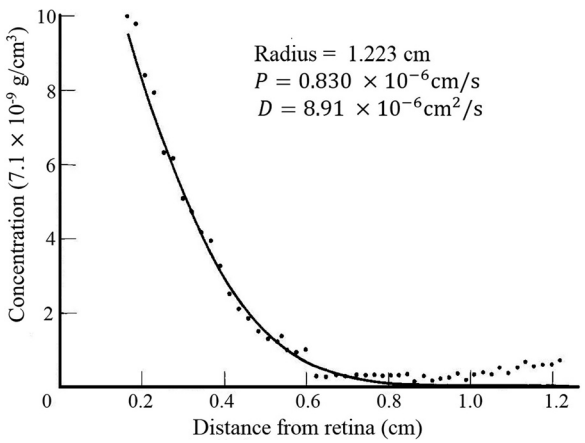

Fig. 2 Concentration of fluorescein in the vitreous versus distance from the retina 1 h after injection. Adapted from Ref. [23], with permission from Springer Nature © 1983.

This is a successful technique that is suitable for in vivo measurements for small molecules that can easily penetrate the BRB. Lower values of P means lower concentration on the vitreous and therefore higher error in detection. Presently, we have started experimentation with direct injection of fluorescein-labeled bevacizumab in rabbit eyes and through-the-lens fluoroscopic imaging. This work is ongoing. Direct injection of MRI contrast agents has also been explored and accurate results have been obtained. We discuss this technique next.

2.2 Nuclear Magnetic Resonance Imaging. Magnetic resonance imaging provides high-quality slice by slice images of the subject and has been found to be an invaluable tool for quantification of physiological transport parameters. The technique relies on solving the inverse problem as the contrast agent diffuses and the MRI provides a snapshot of the concentration profile. With regard to the vitreous humor, Li et al. [26] have carried out experiments with manganese chloride tetrahydrate as a contrast agent. While the aim was to study ion delivery into the eye by transscleral and transcorneal iontophoresis in the rabbit model, they developed some analytical results that are applicable to the diffusion coefficient calculation using experimental data. They injected 100 μl manganese chloride tetrahydrate ($MnCl_2 \cdot 4H_2O$) with a concentration of 1.0 mM in saline into the live-rabbit vitreous and imaging was carried out.

2.2.1 The Inverse Problem. The bolus was assumed to be a sphere of radius a, and in a spherical coordinate system the manganese chloride concentration at a radial distance r from the point of injection was obtained as [26]

$$c(r,t) = c_0\left\{\frac{1}{2}\left[\operatorname{erf}\left(\frac{r+a}{\sqrt{4Dt}}\right) - \operatorname{erf}\left(\frac{r-a}{\sqrt{4Dt}}\right)\right] - \sqrt{\frac{Dt}{\pi r^2}}\left[e^{-\frac{(r-a)^2}{4Dt}} - e^{-\frac{(r+a)^2}{4Dt}}\right]\right\} \tag{7}$$

Specific measurements were carried out over a small volume located around the center of the bolus, and using Eq. (7) with $r = 0$ for various time points over 0–35 min, the value of D was obtained as $(1.3 \pm 0.4) \times 10^{-5}$ cm^2/s. In further work, Molokhia et al. [27] have investigated ocular distribution of a surrogate drug (Galbumin^{TM}, Gd-labeled albumin), again, with the primary aim of iontophoresis in the rabbit model. They injected 100 μl of Galbumin^{TM} and experiments were carried out for initial concentrations of 0.25, 1.0, and 4.0 mg/ml. Following the same procedure as discussed above, the diffusion coefficient was reported to be $(8 \pm 3) \times 10^{-7}$ cm^2/s, close to the estimated coefficient of free diffusion of Galbumin^{TM} in water at 37 °C.

The use of MRI has also been made on artificial tissue (PVA-C hydrogel, see Ref. [28]) for the measurement of the diffusion coefficient of Gd-DTPA, a common medical-use contrast agent with a molecular weight of approximately 1 kDa. While this may only remotely apply to vitreal tissue, we mention it here because of some degree of commonality with the techniques being discussed here. Since they used hydrogel, it could be molded into a desired shape for convenient analysis. The investigators, using 10% PVA-C, shaped it into a parallelepiped with a rectangular cavity to load the contrast agent. The penetration of Gd-DTPA in the vicinity of the flat cavity walls was mathematically described by the one-dimensional diffusion equation so that the concentration could be expressed as

$$c(x,t) = c_0\operatorname{erfc}\left(\frac{x}{\sqrt{4Dt}}\right) \tag{8}$$

where c_0 is the concentration in the cavity and the cavity wall for all time. After imaging at different time points, several different constant concentration contours were tracked, and for each

contour, the x value corresponding to the time point was identified. The x values were plotted against $\sqrt{t}$ with t values as the time points. These plots fell on straight lines where the slope was proportional to $1/\sqrt{D}$, and the best fit gave the value $D = (2.6 \pm 0.3) \times 10^{-6}\text{cm}^2/\text{s}$.

Diffusion of Gd-DTPA in the vitreous has also been studied by Kim et al. [29] who fabricated disk-shaped sustained-release implants, 3.2 mm in diameter and 1.2 mm thick, loaded with Gd-DTPA (Magnevist™, MW 958 Da). Among the goals of the study was to obtain the effective diffusion coefficient of the composite posterior membrane (retina-choroid-sclera membrane). For every experiment, a single disk was surgically implanted in the rabbit eye and both in vivo and ex vivo imaging experiments were carried out. The concentration profile due to the diffusion of the Gd-DTPA from the implant was measured as well as numerically calculated by solving the convection–diffusion equation. The investigators utilized $D = 2.8 \times 10^{-6}\text{cm}^2/\text{s}$ which they attribute to Gordon et al. [28] but the value is slightly different. Through matching numerical simulation with experimental data on the Gd-DTPA distribution, they found the aggregate diffusion coefficient of the retina-choroid-sclera membrane as $6.0 \times 10^{-8}\text{cm}^2/\text{s}$. This is of course more meaningful if as a membrane permeability if divided by the membrane thickness of 0.03 cm to give $P = 2.0 \times 10^{-6}\text{cm}/\text{s}$.

2.2.2 The Contour Method. A very comprehensive measurement technique using MRI has been developed in recent years by Penkova et al. [2] for Gd-DTPA (Magnevist™) and followed up for other gadolinium-based contrast agents by Rattanakijsuntorn et al. [30]. This method is also based on solving the inverse problem, and it entails injecting a drug surrogate (or other gadolinium-labeled drug) into the vitreous of the eye and tracking its spread by MRI. At the same time, a fully analytical model for drug diffusion was employed and the two sets of results (i.e., experimental and theoretical), consisting of spheroidal contours, were matched for various time-points while floating the diffusion coefficient. By minimizing the deviation between theory and experiment (least-squares fit), the diffusion coefficient D was obtained. The work therein relied on the analytical solution of a point source of the drug, and its integration over the domain of the bolus to predict the concentration profile with time. This has necessitated the bolus injection to be of a regular shape, something that has been achieved with very slow injection (2–3 μl/min) of the contrast agent with the use of a syringe pump. While attempts were made to obtain a spherical bolus, it turns out generally spheroidal. This is partly due to the angled needle tip, and additionally as a result of the contrast agent creeping up outside the needle. Even though great care was taken to inject the contrast agent slowly with a syringe pump, complete spherical symmetry has not been possible to achieve. Care was taken to target the bolus at the central region between the lens and the retina, as shown in the schematic in Fig. 3. To obtain a fully analytical solution for the theoretical concentration distribution, the initial bolus was assumed to be a short cylinder, and this approximation turned out to be quite satisfactory after various analytical tests [2]. However, working with the larger molecules (albumin and immunoglobulin), the initial injection boluses are quite distorted and not amenable to the analytical solution. Therefore, a finite element numerical code has been developed for the diffusion process.

2.2.2.1 Methods and Materials. The contour method, originally developed using Gd-DTPA (Magnevist™), has been applied to four different gadolinium-based surrogate drugs (contrast agents) to measure the respective diffusion coefficients in the bovine vitreous humor. Besides Gd-DTPA, these are Prohance™, Gd-Albumin (galbumin™, Biopal), and Gd-Immunoglobulin (IgG, Biopal). The results comparing the first three contrast agents have been published by Rattanakijsuntorn et al. [30] while the results for IgG have been reported by Penkova et al. [35]. To obtain the diffusion coefficient, the following procedure was applied:

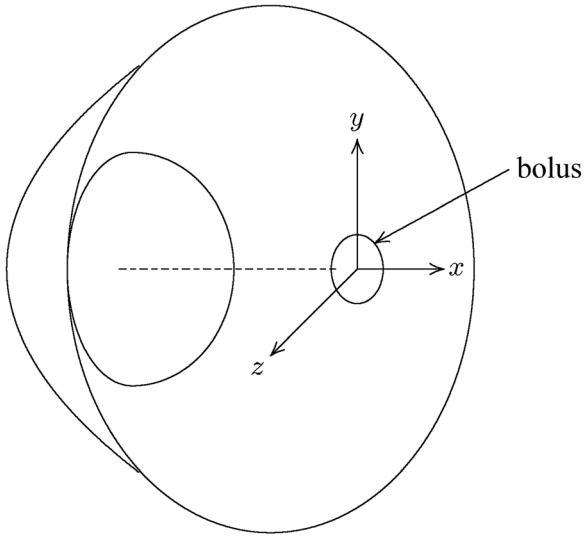

Fig. 3 Coordinate system orientation with respect to the eye. The origin is located at the center of the bolus. Reproduced from Ref. [2], with permission from Elsevier © 2014.

(1) Inject surrogate in the middle of the vitreous region of an ex vivo bovine eye and obtain the concentration distribution by MRI visualization for various time points for that eye.
(2) Develop an analytical (or finite element) solution for the distribution for the initial bolus shape as determined by the first image. For the analytical solution, the initial bolus is taken to be cylindrical in shape [2].
(3) Least-squares fit the experimental concentration contours at different time values with the numerical/analytical ones and deduce the value of the diffusion coefficient D based on the best fit.

2.2.2.2 Apparatus. Fresh bovine eyes (Manning Beef, Pico Rivera, CA) were prepared for MRI by placing them in a 38 mm diameter eye-shaped mold that was custom-fabricated to encase the whole eye. The mold helped maintain shape and wall pressure. For the total time-span considered in this set of experiments, the diffusion front of the contrast agent is well within the walls of the eye, and therefore, the theory and experiment are very close for the total period of the experiment. This allows for reconciliation of theory and experiment to be possible and acquiring a value of D with a relatively high level of accuracy. The contrast agent was injected by means of a syringe pump through a needle guide that snaps onto the tubular eye holder. For each type of contrast agent, 30 μl doses with concentration levels indicated in Table 1 were administered. The respective drug surrogates were injected over a period of 10 min [2] or 15 min [30] with a syringe pump.

The MRI experiments were performed on a 7 Tesla magnet system (Pharmascan, Bruker BioSpin, Germany). Typically, the imaging time for high resolution (192 μm) is 20 min, which is sufficiently low to acquire several temporal images over several hours of diffusion time. The measurements were conducted at 20 °C.

Table 1 Initial injection concentrations of 30 μl injections for the different contrast agents

Drug surrogate	MW (kDa)	Concentration (mg/ml)
Gd-DTPA	0.938	18.76
Prohance	0.559	5.59
Gd-Albumin	74	25.0
Gd-Immunoglobulin	160	25.0

Table 2 Parameters used on the FISP sequence [2]

MRPI parameter	Parameter value
TR (repetition time)	8 ms
TE (echo time)	4 ms
Flip angle	60 deg
Matrix resolution	256 × 256 × 256
Average	4
Scan time	20 min

2.2.2.3 Calibration and Reconstruction. For each contrast agent, phantom tubes were prepared using 0.9% saline solution loaded with various known concentration levels of the contrast agent. The signal intensities from each phantom were plotted against the corresponding concentration values and data-fitted to obtain a calibration curve. As described in Ref. [2], image data was processed with a T1-weighted three-dimensional (3D) gradient echo sequence. The three-dimensional gradient echo sequence sequence uses fast imaging with steady precession (FISP), a steady-state imaging method which allows both the longitudinal and transverse magnetization to reach a dynamic equilibrium [31] when the spin system is excited by a series of RF pulses with a repetition time of TR $\ll$ T2. Strong signals are produced by FISP sequences from tissue with long T2 and short T1, thus enhancing the T1 contrast in tissues. Since the FISP signal becomes independent of T2 when TR$\ll$ T2, sequences can be run with very short TR to reduce the total scan time. In acquiring the preliminary data, the parameters used on the FISP sequence are indicated in Table 2. Signal intensity was sampled over small volumes [$(0.1953\,\text{mm})^3$ voxels] and constructed to give concentration distribution using the calibration curve for the entire vitreous in a cubic grid pattern. It should be noted that since the phantoms accompanied every image, a calibration curve was constructed for every image set. An example of the phantom tubes setup around the eye together with the corresponding calibration curve is given in Fig. 4.

2.2.2.4 Analytical Results. The concentration $m(r,t)$ of the contrast agent based on the point-source solution for an infinite medium is given by

$$m(r,t) = \frac{M}{8(\pi Dt)^{\frac{3}{2}}} e^{-\frac{r^2}{4Dt}} \tag{9}$$

where t is the time, r is the radial distance from the location of the injection, M is the molar amount of the drug deposited, and D is the diffusion coefficient. This expression is based on complete spherical symmetry of the injection, and that the injected volume is small enough to be regarded as a point source. However, as mentioned earlier, it turns out that experimentally, the bolus takes on an ellipsoidal shape. Therefore, the proper representation of the bolus requires the that $m(r,t)$ in Eq. (9) be integrated over the initial bolus volume V' to provide a three-dimensional axisymmetric distribution, i.e.,

$$\begin{aligned} c(r,t) &= \frac{c_0}{8(\pi Dt)^{\frac{3}{2}}} \iiint_{V'} \exp\left(-\frac{|\boldsymbol{r}-\boldsymbol{r}'|^2}{4Dt}\right) dV', \\ &= \frac{c_0}{8(\pi Dt)^{\frac{3}{2}}} \iiint_{V'} \exp\left(-\frac{(x-x')^2+(y-y')^2+(z-z')^2}{4Dt}\right) dV' \end{aligned} \tag{10}$$

where c_0 is the initial bolus concentration. For a spherical bolus, the result of Li et al. [26] given by Eq. (7) is obtained. For the case of an ellipsoidal bolus, the integral in Eq. (10) turned out to be a formidable one for a fully analytical expression. Therefore, as already mentioned, Penkova et al. [2] considered a cylindrical bolus as an approximation to the ellipsoid and found

$$\begin{aligned} c(x,y,z,t) = \frac{c_0}{2} e^{-\frac{(x^2+z^2)}{4Dt}} &\left[\operatorname{erf}\left(\frac{y+a}{\sqrt{4Dt}}\right) - \operatorname{erf}\left(\frac{y-a}{\sqrt{4Dt}}\right)\right] \\ &\times \sum_{n=0}^{\infty} \left\{ \left(\frac{x^2+z^2}{4Dt}\right)^n \frac{1}{n!} \left[1 - e^{-\frac{b^2}{4Dt}} \sum_{k=0}^{n} \frac{1}{k!} \left(\frac{b^2}{4Dt}\right)^k\right]\right\} \end{aligned} \tag{11}$$

where the coordinates (x,y,z) are represented in Fig. 3, $2a$ represents the height of the cylindrical source covering the region $-a \le y \le a$ and b represents the radius. This three-dimensional axisymmetric model was tested for two major analytical concerns: (a) the cylindrical approximation for an ellipsoid, and (b) treating the vitreous as an infinite medium. Penkova et al. [2] have thoroughly examined these items and for (a) the cylindrical approximation, they first tested it against a spherical bolus which has a known exact solution for an infinite medium. It is with the understanding that if the cylindrical bolus can adequately represent a spherical one after some lapsed time, then with some adjustment of the cylinder aspect ratio, an ellipsoid can be represented. The agreement was very good in the vicinity of the bolus, and the comparison of a cylindrical source with $a = b$ yields a concentration distribution very close to a spherical bolus of the same volume. For the ellipsoidal case, the cylinder aspect ratio is approximately in the range, $2 < a/b < 1.5$ depending on each individual case. Color-mapped theoretical images resulting from the cylindrical initial bolus are exhibited in Fig. 5(*b*) and 5(*c*) in Sec. 2.2.2.5 where comparisons with experimental images have been made. In addition, Fig. 5(*c*) includes an image of the cylindrical bolus for the theoretical model in Fig. 5(*b*). These images show that the cylindrical bolus approximation is quite good. For treating the vitreous as an infinite medium [item (b) above], a point source in a spherical shell of radius 2 cm was compared with a corresponding distribution for an infinite medium (Eq. (9)). Also compared was the case of a 2 mm radius spherical bolus in a finite medium with that for an infinite medium. The agreement was excellent within the timeframe of data collection by MRI (2–3 h) using an estimated value of $D = 3.0 \times 10^{-6}\text{cm}^2/\text{s}$. In other words, for the diffusion times considered in the experiments, the vitreous region outside the bolus can be approximated as infinite, giving validity to Eq. (11).

2.2.2.5 Imaging and Data Fitting. After injecting the contrast agent into the middle of the ex vivo bovine vitreous, MR images were taken approximately every 30–45 min. The image data based on signal intensity was converted to concentration values and color-mapped viewing, and additionally, contours of constant intensity were constructed at each time point. Each contour was then least-squares fitted with the corresponding contour obtained from Eq. (11) while the diffusion coefficient D was floated. The best fit thus delivered the value of D. Also, in this process, the aspect ratio a/b of the assumed cylindrical bolus was adjusted to obtain the best fit, and additionally the total mass M (or

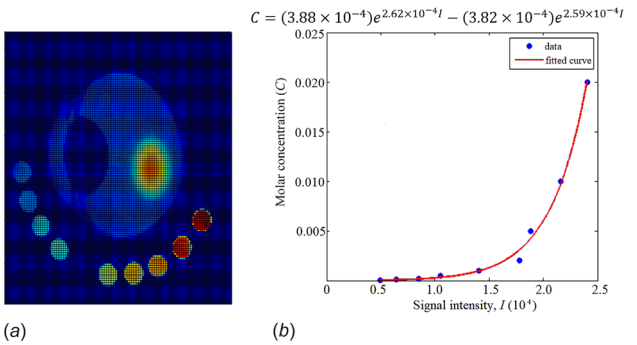

Fig. 4 An example of a color-mapped image of calibration phantom tubes loaded with Gd-DTPA to measured dilution levels surrounding an injected bovine eye, and corresponding fitted calibration curve

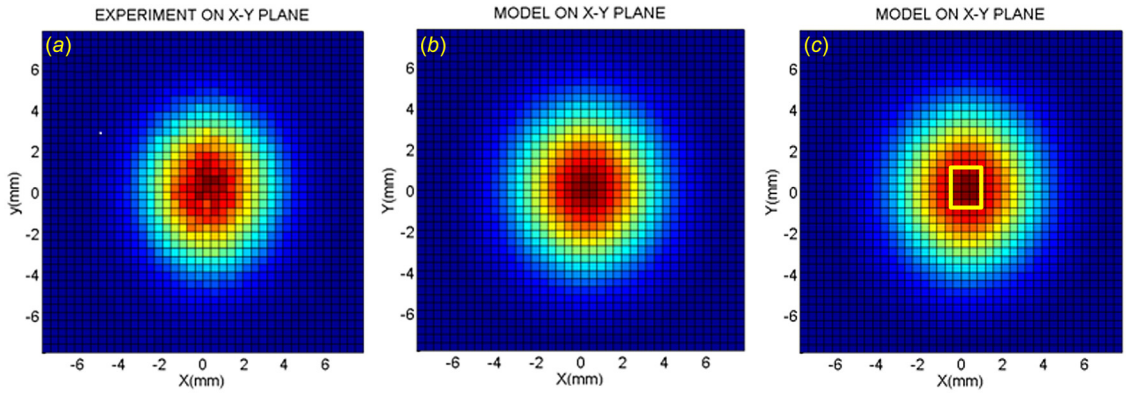

Fig. 5 Colormap of (*a*) experimental and (*b*) theoretical images for Gd-DTPA diffusion in the ex vivo bovine vitreous at 117 min after injection in the *xy*-plane. In (*c*) the initial cylindrical bolus is shown for the theoretical image in (*b*). Adapted from Ref. [2], with permission from Elsevier © 2014.

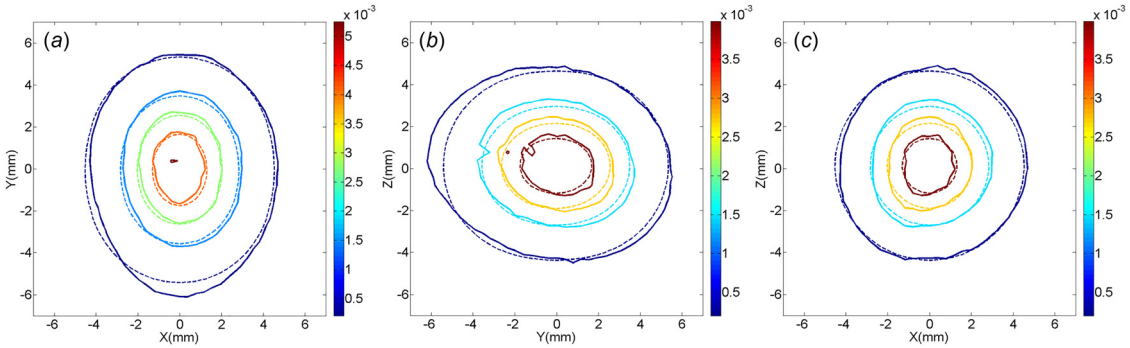

Fig. 6 Contours of constant concentration of Gd-DTPA in the vitreous of the bovine eye. The continuous lines are the experimental results while the broken lines represent the theory according to Eq. (11). The slight indentations seen in (*b*) are the needle marks due to the injection. Adapted from Ref. [2], with permission from Elsevier © 2014.

equivalently, the initial concentration c_0) was floated so that it was constant at every time point. The value of D was initial-guessed and an iterative-corrective procedure was applied to obtain the minimum sum of the squares of the error, i.e.,

$$\text{SSE} = \sum_{i=1}^{N} \left(c_{\text{model},i} - c_{\text{empirical},i}\right)^2 = \text{minimum} \tag{12}$$

where $c_{\text{empirical},i}$ refers to the experimental results at various time points and locations where data has been sampled and $c_{\text{model},i}$ is the corresponding result from Eq. (11). No weighting factor was applied to the squares of the errors. To obtain the minimum sum of the squares of the error, the MATLAB-based simplex search method [32] was used. This is suitable for multidimensional unconstrained minimization. After obtaining the average of the total dispensed surrogate molar mass from each time point, the MATLAB function "fminbnd" (see Refs. [33] and [34]) was then employed to find the optimal diffusion coefficient.

Using three bovine eye samples, and with four to five time points for each eye, the overall average value of the diffusion coefficient was found to be $D = (3.040 \pm 0.274) \times 10^{-6}\text{cm}^2/\text{s}$. With the value of D fully determined, the theoretical contours were drawn over the experimental ones. Also, the theoretical color-maps were obtained for comparison with the experimental ones. Some samples of these results are given here. Figure 6 exhibits contours in the xy, yz, and zx, about the bolus at 117 min after injection. The colormaps in Fig. 5 correspond to the xy plane contour set (a) in Fig. 6.

2.2.2.6 Finite Element Analysis. The mathematical model described in Ref. [2] works very well for the near-symmetric spheroidal distribution profile of drug surrogate, because it was derived from the assumption that the shape of bolus injection is an elongated sphere. In the case of Gd-DTPA, the investigators successfully obtained near-symmetric bolus injection as described above. Similar experiments with Gadoteridol (ProHance$^{\text{TM}}$, $C_{17}H_{29}GdN_4O_7$) have produced near spheroidal shapes in some experiments but some degree of distortion in others. With macromolecules such as Gadolinium–Albumin (Galbumin$^{\text{TM}}$), and Immunoglobulin-Gd (IgG), we found that the shape of concentration distribution was quite distorted. Therefore, the analytical result in Ref. [2] is not suitable for determining diffusion coefficients for these compounds. To accommodate for the nonsymmetric distribution profile, the finite element analysis was implemented for these cases [30].

To model the drug distribution in the vitreous, the three-dimensional mass diffusion equation

$$\frac{\partial c}{\partial t} - D\nabla^2 c = 0 \tag{13}$$

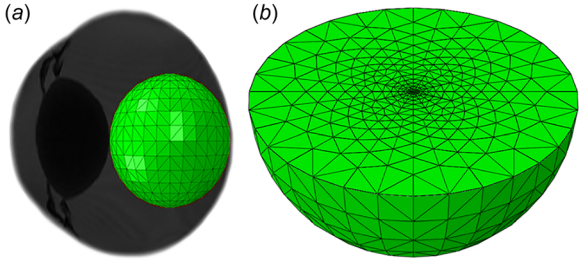

Fig. 7 Finite element tetrahedral mesh. (*a*) The domain of interest; and (*b*) illustration of the finer mesh near the center. Reproduced from Ref. [30], with permission from Creative Commons Attribution 3.0 Unported (CCBY3.0).

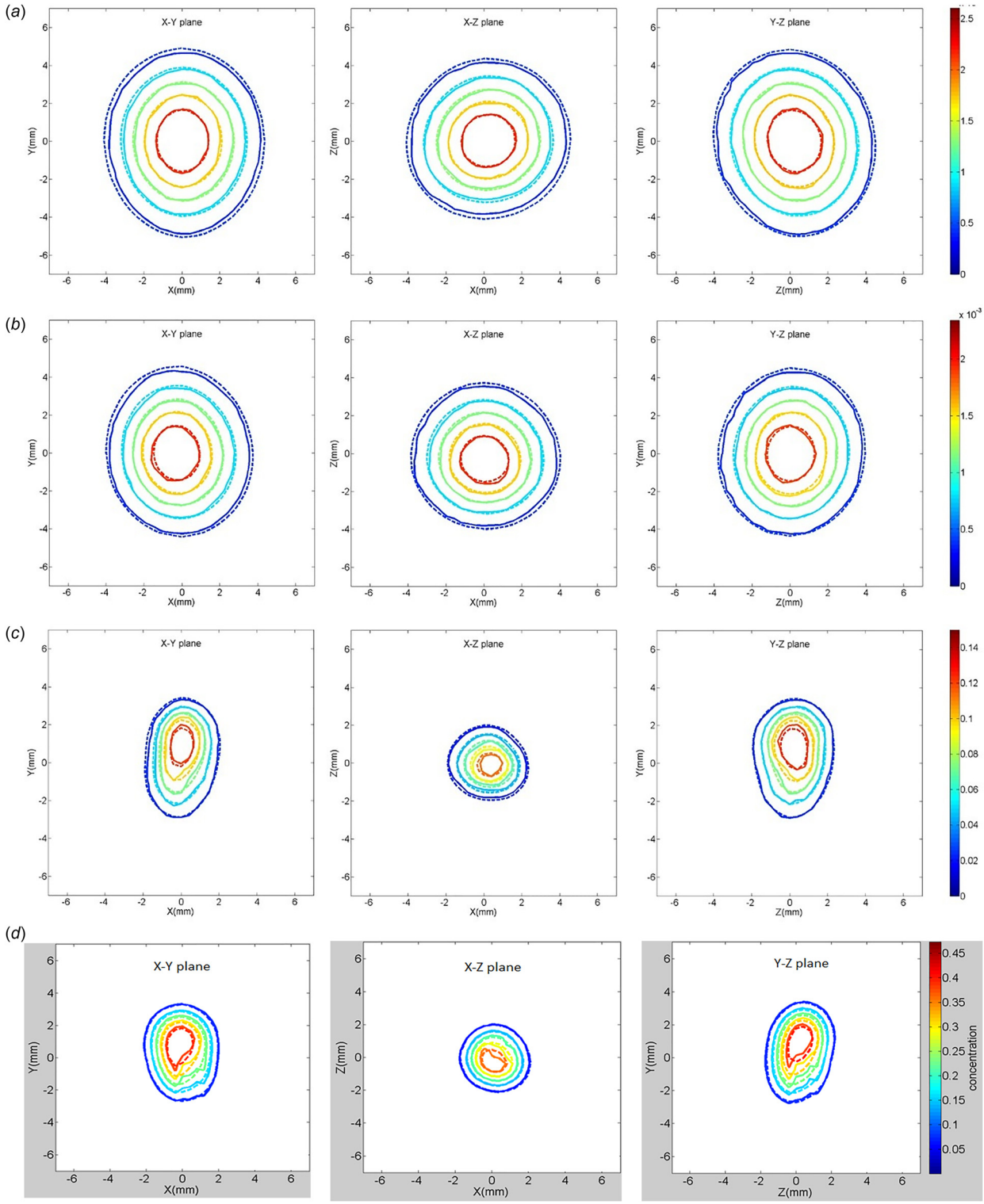

Fig. 8 Contours of constant concentration in (*a*) Gd-DTPA at $t = 85$ min, (*b*) prohance at $t = 88$ min, (*c*) galbumin at $t = 185$ min, and (*d*) IgG at $t = 169$ min (———: measurement, - - - -: finite element analysis). Items (*a*), (*b*), (*c*) adapted from Ref. [30], with permission from Creative Commons Attribution 3.0 Unported (CCBY3.0).

was solved numerically. Since it was already established by Penkova et al. [2] that for the timeframe of the experiments, the effect of the vitreous shape and adjacent tissue is negligible, the domain of interest for the numerical solution was defined as a sphere with a radius of 10 mm as illustrated in Fig. 7(*a*). This geometry was converted into a total of 105,276 finite element tetrahedral meshes using the ABAQUS software. A finer mesh was set up in the region near the center of the sphere since the rate of change of concentration over time near there was larger than the outer region (see Fig. 7(*b*)). The initial condition was based on the concentration of the injected bolus and shape of the bolus as determined by the first MR image. More details are described in Ref. [30]. The finite element code was tested against the exact analytical results for a spherical bolus of radius $r_0 = 2$ mm in a spherical shell of radius $R = 10$ mm as derived in Ref. [2], and found to be in excellent agreement. The data-fitting was carried out in the same

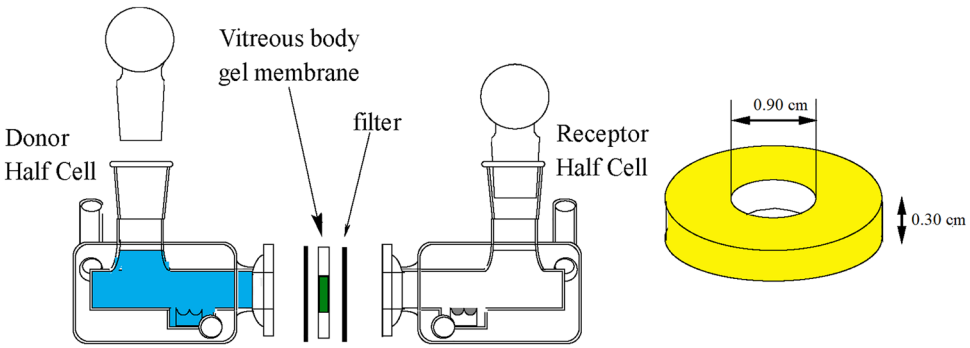

Fig. 9 Schematic of the donor and the receptor chambers for the vitreous diffusion coefficient measurement, with the details of the vitreous humor holder ring. The vitreous cross section area is 0.64 cm^2 and the thickness is 0.3 cm. Courtesy, Ohtori and Tojo [10]; reproduced with permission.

manner as in Ref. [2] and the least-squares fit was based on Eq. (12). The fitted and experimental contours are displayed in Fig. 8 which includes the results for Gd-DTPA (Magnevist^{TM}), ProHance^{TM}, and Galbumin^{TM} as reported by Rattanakijsuntorn et al. [30] with respective diffusion coefficient values $[(3.069 \pm 0.237), (2.739 \pm 0.340), (0.227 \pm 0.021)] \times 10^{-6}$ cm^2/s. It should be mentioned that even for the moderate-sized molecules (Gd-DTPA and Prohance^{TM}), slightly higher accuracy is obtained in matching experimental data with the theoretical predictions using the finite element method for the diffusion equation than the analytical solution. The diffusion coefficient for Gd-DTPA here is slightly higher than that reported by Penkova et al. [2], and additionally has a lower standard deviation. Specifically, for Gd-DTPA, with the analytical cylindrical approximation yields $D = (3.074 \pm 0.27)$ cm^2/s while the finite element method gives (3.07 ± 0.24) cm^2/s. In subsequent experimentation, we carried out measurements with immunoglobulin-gadolinium (IgG) using the same technique [35]. The contours for this case are displayed in Fig. 8(*d*). The diffusion coefficient value for this case is $(2.13 \pm 0.51) \times 10^{-7}$ cm^2/s.

The MRI technique combined with mathematical analysis provides considerable accuracy and allows measurements without having to extract the vitreous. It is applicable to in vivo measurement [26,27] as well, and quite possibly the degree of accuracy achieved in Refs. [2] and [30] may be feasible. Next, we discuss measurements by the disk method.

2.3 Disk Method. Ohtori and Tojo [10] carried out various measurements with dexamethasone sodium *m*-sulfobenzoate (DSMB, molecular weight 0.599 kDa) on in vivo and ex vivo ocular tissue using Japanese albino rabbits. We shall only discuss the segment of their study relevant to the diffusion coefficient of the vitreous humor. They extracted the vitreous from the eye and placed it in a ring of inner diameter 9 mm and 3 mm thickness. The open sides were closed with 0.45 μm membrane filter that allowed DSMB to penetrate through but kept the vitreous contained. The ring was attached on one side to a donor chamber and the other to a receptor chamber, quite like the Ussing chamber system for measuring membrane permeability (see Fig. 9). The donor chamber was filled with DSMB (0.6 mg/ml) while the receptor chamber was filled with fresh phosphate buffer solution (*p*H 7.2). The entire system was maintained at 37 °C by a water jackets around the donor and receptor chambers. Immediately after the start of the experiments, 100 μl samples were taken from the receptor chamber at time intervals of 10 min for the first 20 min, 20 min for the next 160 min, and then every 30 min for the next 2 h. The samples were assayed by high-performance liquid chromatography and concentration values determined. The donor side was not assayed since the concentration change was very small. Based on the total accumulation of DSMB as a function of time, the diffusion coefficient of the vitreous humor was calculated using the solution to the diffusion equation as 5.1×10^{-6} cm^2/s. Further work with this approach was carried out by Tojo et al. [36] on ganciclovir, also for the rabbit vitreous, leading to $D = 9.89 \times 10^{-6}$ cm^2/s.

A similar approach with a simpler tubular cell was taken by Gisladottir et al. [37] for a comparative study of the diffusion coefficient of dexamethasone (molecular weight 0.392 kDa) in porcine vitreous and saline. Their measurement showed $D = (18.06 \pm 6.1) \times 10^{-6}$cm^2/s for the vitreous. The diffusion of fluorescein-Na (molecular weight 0.376 kDa) has also been studied by Nishimura et al. [38] who compared the bovine vitreous in a gel state with a liquefied one. They gave the value for the gel-state vitreous as $D = 4.767 \times 10^{-6}$cm^2/s while in the liquefied state a higher value, 11.007×10^{-6}cm^2/s, was found.

Besides the techniques discussed above, there was one set of results reported for the vitreous by the dynamic light scattering (DLS) method. This work is discussed next.

2.4 Dynamic Light Scattering. The DLS system can measure particle diffusion rates in liquids by Brownian motion. It is therefore useful for measuring the diffusion coefficient of nanoparticles in the vitreous humor. In this regard, Sebag et al. [39] carried out experiments with intact porcine eyes and conducted measurements for the purpose of determining the effect of some degree of liquefaction by microplasmin. They conducted measurements with 18 porcine eyes, with different levels of microplasmin dosage (0, 0.0125, 0.125, 0.25, 0.5, and 0.8 mg). The intact ex vivo eyes were injected with solutions (0.1 ml) of 20 nm polystyrene nanospheres (10 mg/100 ml) along with the dose of

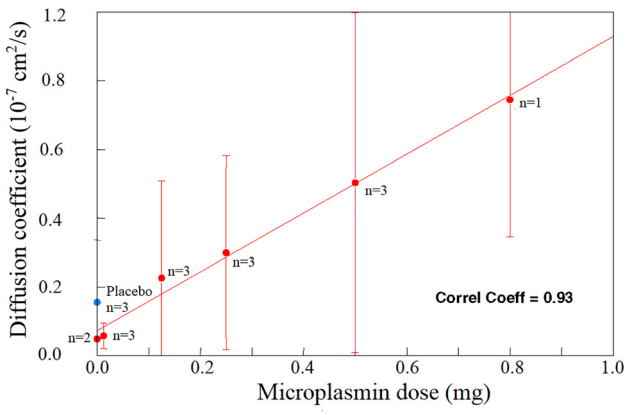

Fig. 10 The diffusion coefficient of 20 nm polystyrene nanospheres as a function of microplasmin dosage. The values *n* refer to the number of porcine eyes used for the specific dose. The placebo corresponds to an injection without mocroplasmin, while zero dose refers to nanoparticles-only injection. Adapted from Ref. [39], with permission from Springer Nature © 2006.

microplasmin. After incubating the eyes at 37 °C for 30 min, the posterior segment was excised and DLS measurements were carried out at numerous points along the optical axis as well from side to side. The results are exhibited in Fig. 10, showing a linear increase in D with microplasmin dosage. For the case without any microplasmin, the diffusion coefficient is seen from the graph as approximately $1 \times 10^{-8}\text{cm}^2/\text{s}$. This work is an excellent illustration of the effect of liquefaction on nanoparticle transport.

3 Discussion

We have presented in this review several sets of results corresponding to the diffusion coefficient of various molecular compounds, as well as nanoparticles in the vitreous humor. We have emphasized the importance of these works, especially in view of comprehensive model development for transport processes in the eye. The focus has been largely on the different measurement techniques and we have discussed imaging with fluorescence and nuclear magnetic resonance, direct measurement with the diffusion chamber and dynamic light scattering. Fluorescence and MRI afford the highest degree of accuracy and at the same time allow imaging the whole eye, in vivo and ex vivo, thus minimizing level of intervention for the measurement. Among the results we have provided in this review includes the diffusion coefficient of fluorescein, and fluorescein-labeled dextran. With MRI, there are of course limitations when dealing with real drugs. For example, with bevacizumab, gadolinium labeling has been difficult to achieve whereas fluorescein labeling with Alexa Fluor 488 dye has been accomplished and is presently being applied to in vivo rabbit eyes. The imaging is being conducted directly through the iris with the HRA+OCT Spectralis and its fluorescein angiography software. Here again, the concentration profile provides the necessary experimental contours which are applicable to the mathematical analysis for the diffusion coefficient measurement. This work is ongoing. Also being explored is measurement of D by radioactive labeling of bevacizumab.

Fluorescence is usually restricted to direct imaging through the lens while MRI covers a much wider range of diffusion snapshots that lead to accurate measurement of the diffusion coefficient. The methods developed with imaging generally rely on a large number of data points and corresponding theory for a least-squares best fit [2,23,28,30] to deliver the unknown diffusion coefficient. The important requirement for imaging-based measurements is that the drug under question needs to be labeled with the contrast agent. For MRI, the preferred contrast element is gadolinium, and labeling with it is not always successful. In addition, the degree of the molecular changes with labeling need to be evaluated since these may affect the transport properties. The use of analytical calculations combined with MR images has provided diffusion coefficient values for manganese chloride tetrahydrate [26], Gd-DTPA [2,30], Gd-labeled albumin [27,30], ProHance™ [30], and gadolinium-labeled immunoglobulin [35].

The disk method employed by Ohtori and Tojo [10], Tojo et al. [36] and Gisladottir et al. [37] uses the diffusion chamber for measuring transport across a cylindrical vitreous body. This technique is useful in that the molecule under question can be directly used and assayed for concentration measurement. The process is delicate since vitreous extraction is required and disturbance to the vitreous body can take place. For further discussion on the diffusion coefficient values obtained in this extensive body of works, we have summarized the results in Table 3 which is ordered by molecular weight. In addition, we present in Fig. 11, a histogram of this table. We see the expected general trend of the inverse relationship between D and the molecular weight. There are some exceptions, however. Prohance™ breaks the trend by having a low value for D in relation to its molecular weight. This has been discussed by Rattanakijsuntorn et al. [30] who compared Prohance™ with Gd-DTPA and made the argument that Prohance™ is nonionic. In another investigation by Gillis et al. [40] on the diffusion coefficient in cartilage, the same trend was found, i.e., D was higher for Gd-DTPA than Prohance™. The other exception is the high value for dexamethasone [37] which seems like an outlier that cannot be explained, and we have not been able to find other data to make a comparison. For galbumin™, Molokhia et al. [27] have reported a substantially higher diffusion coefficient than Rattanakijsuntorn et al. [30]. Here, the former was an in vivo rabbit (therefore at 37 °C) while the latter was for ex vivo bovine eye at 20 °C. Further experimentation is needed for a proper verification. In addition to the histogram, we have in Fig. 12 a log-log plot of the diffusion coefficient versus the molecular weight. Here the outlier dexamethasone is left out. A power-law best fit gives the relationship

$$D = 3.8\,(\text{MW})^{-0.544} \tag{14}$$

where D is in 10^{-6} cm^2/s and MW is in kDa. It is important to note that the molecular weight range 0.1–1.0 kDa has a number of available data points while there are no available results in the 1–74 kDa region. Therefore, some caution needs to be exercised

Table 3 Diffusion coefficient of various compounds in the vitreous humor. The measurements are ex vivo unless noted otherwise.

Authors	Drug/Surrogate	Mol. Wt. (kDa)	Species	Technique	$D(10^{-6}\text{cm}^2/s)$
Li et al. [26]	Manganese chloride tetrahydrate	0.126	rabbit (in vivo)	MRI	13 ± 4
Tojo et al. [36]	Ganciclovir	0.322	Rabbit	Disk method (diffusion chamber)	9.89
Larsen et al. [23]	Fluorescein[1]	0.372	Human (in vivo)	Fluorescence (via BRB)	8.91
Lund-Andersen et al. [25]	Fluorescein	0.372	Human (in vivo)	Fluorescence (via BRB)	9.6 ± 2.0
Lund-Andersen et al. [25]	Fluorescein	0.372	Human (in vivo, diabetic)	Fluorescence (via BRB)	7.4 ± 3.4
Nishimura et al [38]	Fluorescein-Na	0.376	bovine	Disk method(diffusion tube)	4.767
Gisladottir et al. [37]	Dexamethasone	0.392	Porcine	Disk method (diffusion tube)	18.06 ± 6.1
Rattanakijsuntorn et al. [30]	ProHance™	0.559	Bovine	MRI[2]	2.74 ± 0.34
Ohtori and Tojo [10]	DSMB	0.599	Rabbit	Disk method (diffusion chamber)	5.1
Rattanakijsuntorn et al. [30]	Gd-DTPA	0.938	Bovine	MRI[2]	3.07 ± 0.24
Penkova et al. [2]	Gd-DTPA	0.938	Bovine	MRI[2]	3.04 ± 0.27
Molokhia et al. [27]	Galbumin™	74	Rabbit	MRI	0.8 ± 0.3
Rattanakijsuntorn et al. [30]	Galbumin™	74	Bovine	MRI[2]	0.227 ± 0.21
Penkova et al. [35]	Gadolinium-immunoglobulin	160	Bovine	MRI[2]	0.213 ± 0.05
Sebag et al. [39]	20 nm nanospheres	—	Porcine	DLS	0.01
Sebag et al. [39]	20 nm nanospheres	—	Porcine with microplasmin	DLS	0.01–0.15

[1]Reported molecular weight of fluorescein is 372 Da [23].
[2]Measurements are at room temperature (20 °C).

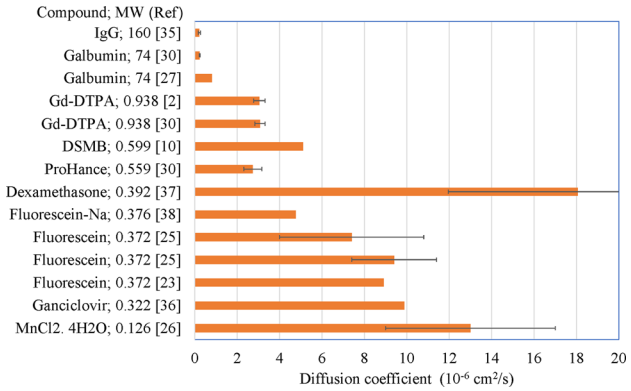

Fig. 11 Comparison of the diffusion coefficients for various molecular weights. The horizontal axis is the diffusion coefficient D (10^{-6} cm^2/s). This histogram is based on diffusion coefficient values reported by various authors as per Table 3. For cases where the uncertainty was not reported, we do not include error bars.

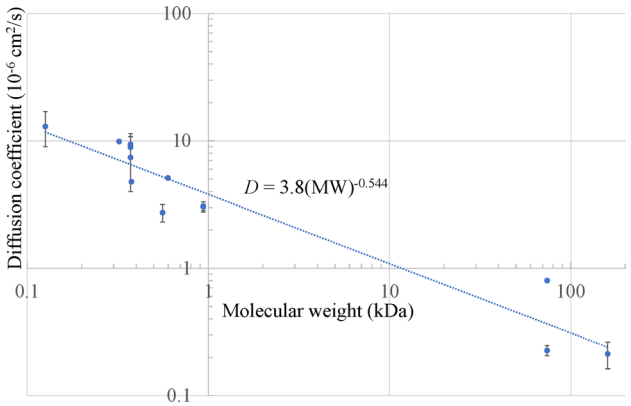

Fig. 12 A log-log plot of diffusion coefficient versus molecular weight with a power-law best fit

in interpreting the fitted formula given in Eq. (14). Keeping this in mind, we have plotted the dataset in the 0.1–1.0 kDa range. The set of reported measurements in this range leads to the plot given in Fig. 13 where both axes are on a linear scale. The best fit (again without dexamethasone) in this range yields

$$D = -5.37\ln(\mathrm{MW}) + 2.236 \tag{15}$$

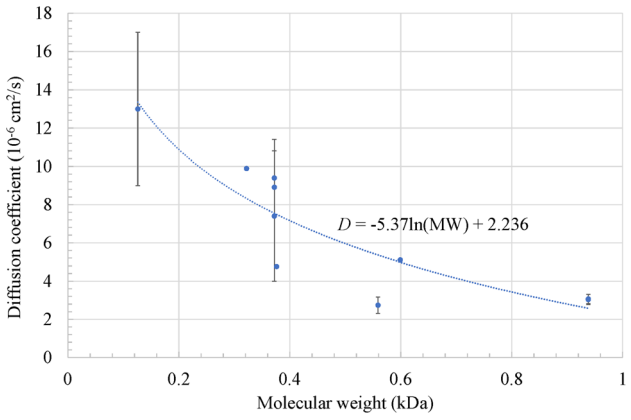

Fig. 13 Plot of diffusion coefficient versus molecular weight in the range 0.1–1.0 kDa with a logarithmic best fit

where the units are as noted for Eq. (14). For both the plots some of the data points do not have error bars because the uncertainty in those cases was not reported. It should also be noted that the diffusion coefficient results have been data-fitted with corresponding molecular masses, and other factors (such as effects of charge) are not included. Also, in creating the correlations (14) and (15) the different mammal species have not been taken into consideration since the overall dataset is quite limited for the vitreous humor.

The various sets of results presented here provide a fairly exhaustive summary of the state of the art for measuring the diffusion coefficient of different materials in the vitreous humor. The imaging techniques offer a high degree of accuracy provided the drug in question can be labeled with a contrast agent. DLS is another approach that has been little explored. The method used by Sebag et al. [39] provides considerable potential for macromolecules and nanoparticles.

Funding Data

- National Eye Institute under the NIH Grant No. 5R01EY026599.

Nomenclature

Symbols

a = spherical bolus radius cylindrical bolus half-height
b = cylindrical bolus radius
c = drug concentration
c_0 = initial drug concentration
D = diffusion coefficient
M = total molar mass of drug in a point source
$m(r,t)$ = drug concentration due to a point source
MW = molecular weight
P = membrane permeability (cm/s)
R = radius of curvature of eye posterior (Fig. 1)
t = time
x, y, z = Cartesian coordinates

Acronyms

BRB = blood-retinal barrier
DLS = dynamic light scattering
DTPA = diethylenetriamine pentaacetic acid
DSMB = dexamethasone sodium *m*-sulfobenzoate
FD = fluorescein-labeled dextran
FISP = fast imaging with steady precession
HRA = Heidelberg retinal angiography
MRI = magnetic resonance imaging
OCT = optical coherence tomography
PVA-C = polyvinyl alcohol cryogel

References

[1] Duvvuri, S., Majumdar, S., and Mitra, A., 2003, "Drug Delivery to the Retina: Challenges and Opportunities," Expert Opin. Biol. Ther., **3**(1), pp. 45–56.
[2] Penkova, A., Rattanakijsuntorn, K., Sadhal, S., Tang, Y., Moats, R., Hughes, P. M., Robinson, M. R., and Lee, S. S., 2014, "A Technique for Drug Surrogate Diffusion Coefficient Measurement by Intravitreal Injection," Int. J. Heat Mass Transfer, **70**, pp. 504–514.,"
[3] Lee, T., and Robinson, J., 2004, "Drug Delivery to the Posterior Segment of the Eye III: The Effect of Parallel Elimination Pathway on the Vitreous Drug Level After Subconjunctival Injection," J. Ocul. Pharmacol. Ther., **20**(1), pp. 55–64.
[4] Haghjou, N., Abdekhodaie, M., Cheng, Y., and Saadatmand, M., 2011, "Computer Modeling of Drug Distribution After Intravitreal Administration," World Acad. Sci. Eng. Technol., **77**, pp. 706–716.
[5] Stay, M., Xu, J., Randolph, T., and Barocas, V., 2003, "Computer Simulation of Convective and Diffusive Transport of Controlled-Release Drugs in the Vitreous Humor," Pharm. Res, **20**(1), pp. 96–102.
[6] Balachandran, R., 2010, "Computational Modeling of Drug Transport in the Posterior Eye," Ph.D. dissertation, University of Minnesota, Minneapolis, MN.
[7] Balachandran, R., and Barocas, V., 2008, " Computer Modeling of Drug Delivery to the Posterior Eye: Effect of Active Transport and Loss to Choroidal Blood Flow," Pharma. Res., **25**(11), pp. 2685–2696.
[8] Kathawate, J., and Acharya, S., 2008, "Computational Modeling of Intravitreal Drug Delivery in the Vitreous Chamber With Different Vitreous Substitutes," Int. J. Heat Mass Transfer, **51**(23–24), pp. 5598–5609.

[9] Kim, S., Lutz, R., Wang, N., and Robinson, M., 2007, "Transport Barriers in Transscleral Drug Delivery for Retinal Diseases," Ophthalmic Res., **39**(5), pp. 244–254.
[10] Ohtori, A., and Tojo, K., 1994, "In Vivo/In Vitro Correlation of Intravitreal Delivery of Drugs With the Help of Computer Simulation," Biol. Pharm. Bull., **17**(2), pp. 283–290.
[11] Li, S. K., Hao, J., Liu, H., and Lee, J. H., 2012, "MRI Study of Subconjuctival and Intravitreal Injections," J. Pharm. Sci., **101**(7), pp. 2353–2363.
[12] Li, S. K., Lizak, M. J., and Jeong, E., 2008, "MRI in Ocular Drug Delivery," NMR Biomed., **21**(9), pp. 941–956.
[13] Siggers, J., and Ethier, C., 2012, "Fluid Mechanics of the Eye," Ann. Rev. Fluid Mech., **44**(1), pp. 347–372.
[14] Vafai, K., 2011, *Porous Media: Applications in Biological Systems and Biotechnology*, CRC Press, Boca Raton, FL.
[15] Mukundakrishnan, K., and Ayyaswamy, P., 2011, "Fluid Mechanics: Transport and Diffusion Analyses as Applied in Biomaterials Studies," *Comprehensive Biomaterials*, P. Ducheyne, K. Healy, D. Hutmacher, D. Grainger, and C. Kirkpatrick, eds., Vol. 3, Elsevier, Amsterdam, The Netherlands, pp. 133–153.
[16] Khanafer, K., and Vafai, K., 2006, "The Role of Porous Media in Biomedical Engineering as Related to Magnetic Resonance Imaging and Drug Delivery," Heat Mass Transfer, **42**(10), pp. 939–953.
[17] Truskey, G., Yuan, F., and Katz, D., 2009, *Transport Phenomena in Biological Systems*, 2nd ed., Pearson Prentice Hall, New York.
[18] Cunha-Vaz, J., and Maurice, D., 1969, "Fluorescein Dynamics in the Eye. Documenta Ophthalmologica," Adv. Ophthalmol., **26**, p. 61.
[19] Kaiser, R. J., and Maurice, D. M., 1964, "The Diffusion of Fluorescein in the Lens," Exper. Eye Res., **3**(2), pp. 156–165.
[20] Araie, M., and Maurice, D. M., 1991, "The Loss of Fluorescein, Fluorescein Glucuronide and Fluorescein Isothiocyanate Dextran From the Vitreous by the Anterior and Retinal Pathways," Exper. Eye Res., **52**(1), pp. 27–39.
[21] Garlick, D., and Renkin, E., 1970, "Transport of Large Molecules From Plasma to Interstitial Fluid and Lymph in Dogs," Amer. J. Physiol., **219**(6), pp. 1595–1605.
[22] Maurice, D. M., 1987, "Flow of Water Between Aqueous and Vitreous Compartments in the Rabbit Eye," Amer. J. Physiol., **252**, pp. Fl04–Fl08.
[23] Larsen, J., Lund-Andersen, H., and Krogsaa, B., 1983, "Transient Transport Across the Blood-Retinal Barrier," Bull. Math. Biol., **45**(5), pp. 749–758.
[24] Lund-Andersen, H., Krogsaa, B., and Jensen, P. K., 1982, "Fluorescein in Human Plasma In Vivo," Acta Ophthalmol., **60**(5), pp. 709–716.
[25] Lund-Andersen, H., Krogsaa, B., la Cour, M., and Larsen, J., 1985, "Quantitative Vitreous Fluorophotometry Applying a Mathematical Model of the Eye," Invest. Ophthalmol. Vis. Sci., **26**, pp. 698–710.
[26] Li, S., Jeong, A., and Hastings, M., 2004, "Magnetic Resonance Imaging Study of Current and Ion Delivery Into the Eye During Transscleral and Transcorneal Iontophoresis," Invest. Ophthalmol. Vis. Sci., **45**(4), pp. 1224–1231.
[27] Molokhia, S., Jeong, E.-K., Higuchi, W., and Li, S., 2009, "Transscleral Iontophoretic and Intravitreal Delivery of a Macromolecule: Study of Ocular Distrubution In Vivo and Postmortem With MRI," Exper. Eye Res., **88**(3), pp. 418–425.
[28] Gordon, M. J., Chu, K. C., Margaritis, A., Martin, A. J., Ethier, C. R., and Rutt, B. K., 1999, "Measurement of Gd-DTPA Diffusion Through PVA Hydrogel Using a Novel Magnetic Resonance Imaging Method," Biotech. Bioeng., **65**(4), pp. 459–467.
[29] Kim, H., Lizak, M. J., Tansey, G., Csaky, K. G., Robinson, M. R., Yuan, P., Wang, N. S., and Lutz, R. J., 2005, "Study of Ocular Transport of Drugs Released From an Intravitreal Implant Using Magnetic Resonance Imaging," Ann. Biomed. Eng., **33**(2), pp. 150–164.
[30] Rattanakijsuntorn, K., Penkova, A., and Sadhal, S. S., 2018, "Mass Diffusion Coefficient Measurement for Vitreous Humor Using FEM and MRI," IOP Conf. Ser.: Mat. Sci. Engin., **297**, p. 012024.
[31] Liang, Z.-P., and Lauterberg, P., 2000, *Principles of Magnetic Resonance Imaging: A Signal Processing Perspective* (IEEE Press Series in Biomedical Engineering), Wiley, Hoboken, NJ.
[32] Lagarias, J. C., Reeds, J. A., Wright, M. H., and Wright, P. E., 1998, "Convergence Properties of the Nelder-Mead Simplex Method in Low Dimensions," SIAM J. Optim., **9**(1), p. 112.
[33] Forsythe, G. E., Malcolm, M. A., and Moler, C. B., 1977, *Computer Methods for Mathematical Computations*, Prentice Hall, Englewood Cliffs, NJ.
[34] Brent, R., 1973, *Algorithms for Minimization Without Derivatives*, Prentice Hall, Englewood Cliffs, NJ.
[35] Penkova, A. N., Rattanakijsuntorn, K., Khoobyar, A., Moats, R., Fraser, S., Humayun, M. S., and Sadhal, S. S., 2018, "Gadolinium-Immunoglobilin Study for Diffusion Coefficient Measurement of Bovine Vitreous Humor for Drug Delivery Modeling," Invest. Ophthalmol. Vis. Sci., **59**(9), p. 4457.
[36] Tojo, K., Nakagawa, K., Morita, Y., and Ohtori, A., 1999, "A Pharmacokinetic Model of Intravitreal Delivery of Ganciclovir," Eur. J. Pharma. Biopharma., **47**(2), pp. 99–104.
[37] Gisladottir, S., Loftsson, T., and Stefansson, E., 2009, "Diffusion Characteristics of Vitreous Humour and Saline Solution Follow the Stokes Einstein Equation," Graefe's Arch. Clin. Exper. Ophthalmol. (Albrecht Von Graefes Archiv Für Klinische Und Experimentelle Ophthalmologie), **247**(12), pp. 1677–1684.
[38] Nishimura, Y., Hayashi, H., Oshima, K., and Iwata, S., 1986, "Alteration of Diffusion Velocity of Fluorescein-Na in Dependence on Vitreous Liquefaction," Jpn. J. Ophthalmol., **90**(11), pp. 1313–1316.
[39] Sebag, J., Ansari, R., and Suh, K., 2007, "Pharmacologic Vitreolysis With Microplasmin Increases," Graefe's Arch. Clin. Exper. Ophthalmol., **245**(4), pp. 576–580.
[40] Gillis, A., Gray, M., and Burstein, D., 2002, "Relaxivity and Diffusion of Gadolinium Agents in Cartilage," Magn. Reson. Med., **48**(6), pp. 1068–1071.